

1 Brief communication: Mountain permafrost acts as an aquitard 2 during an infiltration experiment monitored with ERT time- 3 lapse measurements

4 Mirko Pavoni¹, Jacopo Boaga¹, Alberto Carrera², Giulia Zuecco³, Luca Carturan³ and Matteo Zumiani⁴

5 ¹ Department of Geosciences, University of Padova, Padua, Italy

6 ² Department of Agronomy, Food, Natural Resources, Animals and Environment, University of Padova, Legnaro (PD), Italy

7 ³ Department of Land, Environment, Agriculture and Forestry, University of Padova, Legnaro (PD), Italy

8 ⁴ Servizio Geologico, Provincia Autonoma di Trento, Italy

9

10 *Correspondence to:* Mirko Pavoni (mirko.pavoni@phd.unipd.it)

11 **Abstract.** Frozen layers within the subsurface of rock glaciers are generally assumed to act as aquicludes or aquitards. So far,
12 this behavior was mainly defined by analyzing the geochemical characteristics of spring waters. In this work, for the first time,
13 we experimentally confirmed this assumption by executing an infiltration test in a rock glacier of the Southern Alps, Italy.
14 Time-lapse electrical tomography (ERT) technique monitored the infiltration of 800 liters of salt-water released on the surface
15 of the rock glacier. 24 hours ERT monitoring highlighted that the injected water was not able to infiltrate into the underlying
16 frozen layer.

17 1 Introduction

18 In alpine regions, groundwater originating from moraines and rock glaciers is highly contributing to the streamflow (Wagner
19 et al. 2016). Therefore, a key factor in the hydrological modeling of alpine catchments is the determination of the hydraulic
20 properties of these landforms. The subsoil hydrodynamic of moraines, talus and hillslope aquifers is relatively well known,
21 but the hydraulic behavior of rock glaciers and their impact on the hydrology of alpine catchments are relatively less defined
22 (Pauritsch et al., 2017 and references therein). The hydrological and geochemical monitoring of active rock glaciers springs
23 was successfully used to investigate runoff processes and presence of frozen layer in alpine catchments (e.g., Krainer et al.,
24 2007; Carturan et al. 2016). In active or ice-rich intact rock glaciers, continuous frozen layers are typically considered as
25 aquicludes (Giardino et al., 1992). Krainer et al. (2007) separated a subsurface flow component, derived from snow-ice melting
26 and rainwater, and a deeper and longer stored aquifer at the bottom of the Reichenkar active rock glacier (Austrian Alps).
27 Harrington et al. (2018) defined the inactive Helen Creek rock glacier (Alberta, Canada) as an unconfined aquifer, as the
28 limited ground ice distribution is unlikely to act as a pure aquiclude. These investigations suggest that rock glaciers host
29 complex and heterogeneous aquifers with a layered internal structure. Nevertheless, geochemical surveys have not the ability
30 to accurately define the aquifer's structure (e.g., layers thickness, discontinuities, and lateral/vertical heterogeneities) if not
31 integrated with geophysical surveys.

32 To verify and confirm the hydraulic behavior of the frozen layer, we tested an infiltration experiment combined with electrical
33 resistivity tomography (ERT) time-lapse measurements in the Sadole rock glacier (Southern Alps, Italy). Controlled irrigation
34 experiments combined with ERT time-lapse measurements were successfully applied to study the vadose zone (Cassiani et al.,
35 2006), and even more challenging hillslope catchments (Cassiani et al., 2009). The Sadole rock glacier infiltration experiment
36 represents the first attempt to adopt this monitoring technique to the mountain permafrost environment. Considering the
37 promising results, the experiment can be used as reference to improve future tests and better characterize the hydraulic
38 properties of the frozen subsoils.

39 **2 Site description**

40 The Sadole rock glacier is located in the Sadole Valley, in the Eastern part of the Trento Province (North-East Italy, Fig.1A).
41 The rock glacier altitude ranges between 1820 m a.s.l. and 2090 m a.s.l. It is a complex periglacial landform made by the
42 confluence of three different lobes (Fig.1B), which developed on two coalescent glacial cirques. Steep rock walls and sharp
43 crests almost entirely bound these cirques, except for the Sadole Pass that was likely a glacial transfluence saddle during the
44 last glaciation. Slope deposits are found between the rock walls and the rock glacier rooting areas. These deposits have
45 gravitational or mixed gravitational/debris-flow/avalanche origin and are predominantly active. From a geological point of
46 view, the rock glacier is composed of magmatic rocks (riodacitic ignimbrites) that belong to the Athesian Volcanic Group, a
47 late-Paleozoic (Permian) volcanic succession. The Sadole rock glacier is classified as ‘relict’ in the inventory of Trento
48 Province (Seppi et al., 2012), in agreement with the guidelines provided by the IPA Action Group (RGIK, 2022). Despite this,
49 the general convex morphology and the low water temperature of its springs (ranging between 1.0 and 1.8°C), suggested that
50 this rock glacier may preserve permafrost (Carturan et al., 2016 and references therein). In addition, ice outcrops were observed
51 in the mid-summer two meters below the surface, in a pit dug during the 1st World War (green dot in Fig.1B). Several ERT
52 transects (blue, violet, and brown lines in Fig.1B) were collected in summer 2021 on the rock glacier, confirming the presence
53 of a discontinuous frozen layer (see high resistivity areas in Figs.1D-E). Soil temperature sensors (red dots in Fig.1B) were
54 installed in different location of the rock glacier bodies. Finally, to evaluate the hydraulic behavior of the frozen layer, an
55 infiltration experiment with ERT time-lapse measurements was realized in middle June 2022. The ERT monitoring transect
56 (red line in Fig.1C) was in the same area of the ERT surveys 2021, considering the maximum slope gradient. The line was
57 placed to detect how the injected water flows in the area where the frozen layer is present, and how it flows where the frozen
58 layer ends.

59 **3 Methods**

60 **3.1 Experiment principles**

61 ERT surveys are performed to detect the electrical properties of the ground. The method can be used for monitoring time-
62 dependent subsurface processes by repeating periodically the measurements using the same electrode array (Binley, 2015).
63 This ERT data acquisition method is defined as “ERT time-lapse technique”, and can be performed with controlled irrigation
64 experiments (Cassiani et al., 2006; Cassiani et al., 2009). In these tests, a large amount of salt-water is released into the subsoil
65 system, and the propagation of the injected water is investigated using the ERT time lapse survey. An ERT dataset is collected
66 before the injection, at a time called time zero (t_0). Subsequently, as the salt water propagates into the ground, new datasets
67 are periodically acquired at defined time steps (t_1, t_2, \dots, t_n). The changes of electrical properties in the subsoil, due to the
68 injected water flow, are usually not clearly highlighted by comparing the individual inverted resistivity models. To enhance
69 the variation from one-time step to the next, only the inverted model t_0 is represented in terms of absolute resistivities, while
70 the other time steps are plotted in terms of percentage variations of resistivity with respect to the t_0 model (Binley, 2015).

71 **3.2 Data acquisition**

72 An ERT survey line of 72 electrodes, spaced 1.5 meters from each other (total length of 106.5 meters), was centered with
73 respect to the discontinuous frozen layer detected in the 2021 ERT surveys. The injection point was placed in the middle of
74 the array. The measurements were performed with a Syscal Pro georesistivimeter (Iris Instruments), using a dipole-dipole
75 configuration with different skips (1, 3, 5 and 7 - the skip represents the number of electrodes skipped to create a dipole), and
76 a stacking range between 3 and 6, with 5% error threshold. The chosen configuration allowed to collect direct and reciprocals
77 measurements and to estimate a reliable experimental error for the acquired datasets (Binley, 2015). The position,
78 characteristics of the survey line, and the acquisition scheme, were defined to better highlight the flow of the injected water.

79 The array setup with relatively short spacing and low skip number guarantees a good resolution in the shallower subsurface,
80 while the setup with higher skip number provides a greater penetration depth due to the total length of the array. Furthermore,
81 a very large number of measuring points (2594) were acquired to increase the possibility of detecting resistivity variations in
82 the subsurface due to water flow. With this high number of measured points, the characteristics of the array and the acquisition
83 scheme, we aimed to increase the reliability of our models even in areas where the sensitivity is notoriously low (e.g., the
84 bottom and the edges, Binley, 2015).

85 The ERT data quality in rock glacier environments is usually low due to the high contact resistances between electrodes and
86 boulders (Hauck & Kneisell, 2008). To partially overcome this problem, and increase the amount of injected current (Pavoni
87 et al., 2022), we inserted the electrodes between the boulders using sponges soaked with saltwater (Fig.2A). The sponges were
88 wetted at the beginning of each measurement during the ERT time lapse survey, to reach (approximately) homogeneous contact
89 resistances for each collected dataset. Collecting measurements with different contact resistances could lead in fact to changes
90 in resistivity models not linked to the flow of the injected water.

91 The water for the experiment was collected during the previous months, using ten 100-liter bins. The bins were placed on the
92 Sadole rock glacier in the point selected for the water injection, in the early spring when snow cover was still present (Fig.B).
93 They were filled with snow and covered with nylon sheets pierced at their center to collect rainwater. This way, in mid-June
94 the bins were completely filled with a mixture of snowmelt and rainwater. Before the experiment, 3 kg of NaCl were added to
95 each bin to obtain a salt-water solution. After collecting the t_0 dataset, 8 bins were emptied one after the other, injecting 800
96 liters of salt-water into the subsurface system (Fig.2C). Four datasets were acquired in the first hour, followed by four datasets
97 at hourly intervals, and a last dataset was collected 24 hours after water injection. No rain or uncontrolled water contribution
98 happened during the experiment.

99 **3.3 Data processing**

100 The acquired datasets were filtered removing quadrupoles with a stacking error higher than 5%, and a reciprocal error higher
101 than 20%. Only the common quadrupoles saved in all the filtered datasets were used to perform the inversion process of each
102 dataset. The inversion modeling was performed using the Python-based software ResIPy (Blanchy et al., 2020), and an
103 expected data error of 20% was defined according to the reciprocal check (Binley, 2015). Once a common unstructured
104 triangular mesh was created, all the acquired datasets were inverted independently. Only the t_0 initial model is here plotted in
105 terms of absolute electrical resistivity values (logarithmic scale), while the other models (t_n) obtained with the ERT time-lapse
106 survey are plotted as percentage variations in resistivity compared to the initial model t_0 . In order to avoid emphasizing changes
107 in the high resistivity zone, the percentage variations in resistivity were calculated using logarithmic values. Since we defined
108 an expected data error of 20%, tiny resistivity changes in the inverted tomograms are considered not reliable to highlights the
109 flow of the injected water. Therefore, in the time-lapse models, negative resistivity variations lower than 10% are plotted in
110 light gray color. Finally, to detect the frozen layer boundary in t_0 model, we applied the steepest gradient method (Chambers,
111 2012). This method, as suggested by forward modeling analysis, is the most reliable to evaluate the thickness of the active
112 layer (Herring et al., 2022).

113 **4 Results**

114 Figure 3A shows the t_0 resistivity section. The high resistivities ($\rho > 30 \text{ k}\Omega\text{m}$) close to the surface are linked to the voids among
115 coarse debris and blocks, typical in rock glacier environments (Hauck and Kneisel, 2008). Below this high resistivity layer,
116 lower values of resistivity ($\rho < 10 \text{ k}\Omega\text{m}$) are found and can be associated with a decrease in porosity and grain size of the deposit,
117 and a possible increase in humidity. At the south-west and north-east edges of the section this low resistivity layer reaches the
118 bottom of the model. On the other hand, in the central part of the model ($30 < x < 70 \text{ m}$) a clear change is detected at a depth of
119 about 10 meters. Below this boundary, the resistivity rapidly increases ($\rho > 50 \text{ k}\Omega\text{m}$), highlighting the presence of a frozen layer

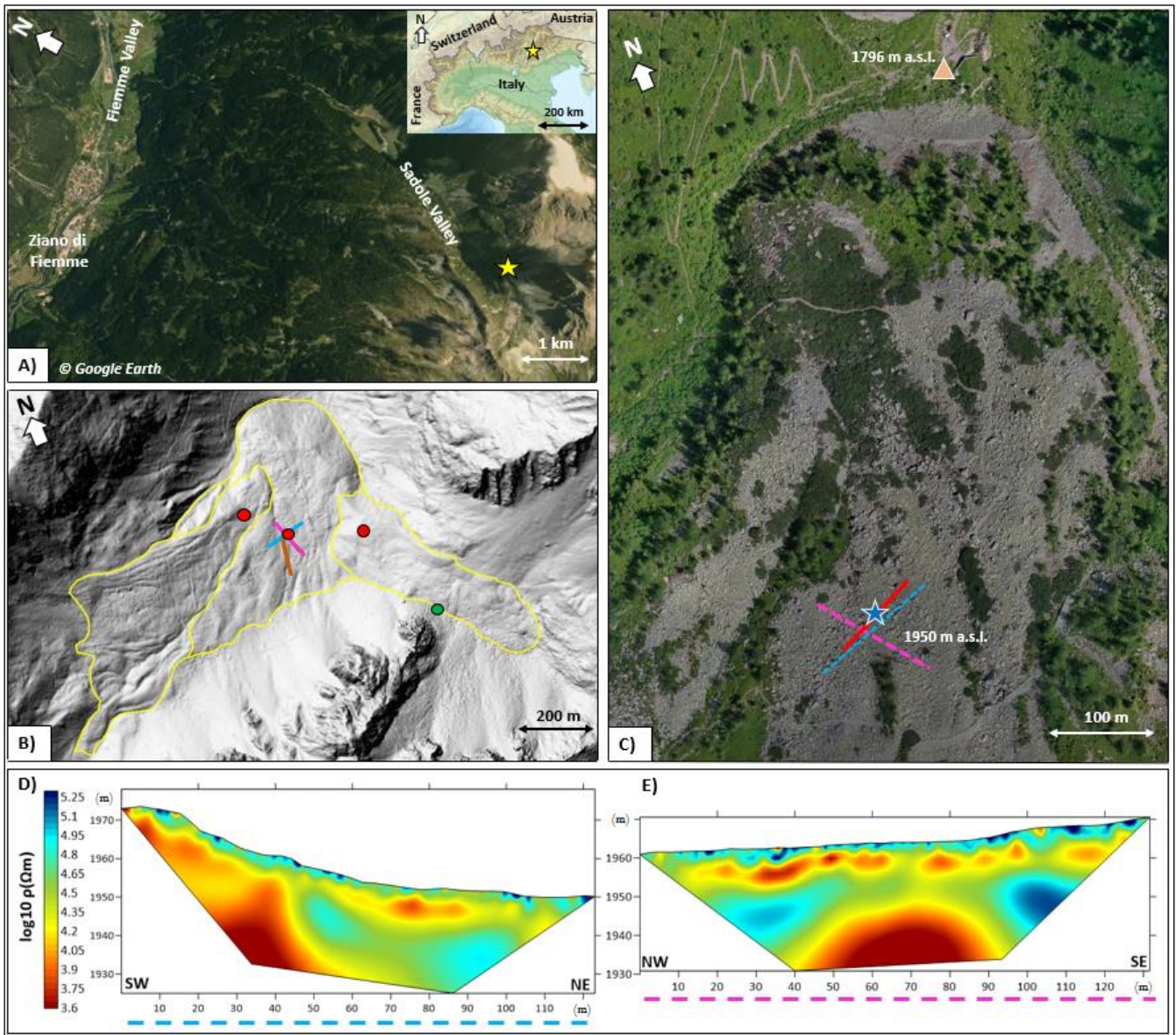
120 (Hauck and Kneisell, 2008). By applying the steepest gradient method in the vertical direction, we defined 55 k Ω m as the
121 upper boundary of the permafrost layer, and the same value was used to define its lateral termination.
122 In Fig. 3B high negative resistivity variations (>20%) show a quick vertical infiltration of the injected water up to a depth of
123 10 meters within the first 15 minutes after the injection. This wet area persisted below the injection point until the last survey
124 t10 (Fig.3M), even if it seems to slowly shrink from one data acquisition to the next. Negative resistivity variations in Figs.
125 3B-E indicate a downslope subsurface flow in the north-east direction above the identified frozen layer. Where the frozen layer
126 ends ($x \approx 70$ m), the water clearly appears to be able to propagate deeper vertically. Concerning the upslope area ($x < 30$ m),
127 the negative resistivity variations are found from the surface to the bottom of the section until t4 (Fig.3B-3F), highlighting a
128 main vertical infiltration of the injected water. In the following time steps the negative values develop mainly at few meters of
129 depth (Figs. 3F-3L), indicating a possible anomalous upslope subsurface flow (south-west direction). These negative
130 variations, upslope of the injection area, are still present after 24 hours (t10, Fig. 3M) but, at the same time, the water still
131 flows downslope in the north-east direction. On the other hand, negative resistivity variations are practically null inside the
132 defined frozen layer, suggesting that the injected water did not propagate through it.

133 **4 Discussion and conclusions**

134 High negative resistivity variations (>20%) observed for t1 close to the injection area indicate a rapid vertical infiltration of
135 the water due to the presence of boulders, voids, fractures, and coarse sediments with high vertical permeability. The large
136 amount of injected water has probably saturated this area, which has become the source of the subsurface flow. Although we
137 do not have any measurements of saturated hydraulic conductivity, we can speculate that hydraulic conductivities may be
138 much higher (in the order of 10^{-2} m/s) than those ones observed in shallow soil layers of young moraines, as found in the Swiss
139 Alps by Maier et al. (2021). Subsurface flow, moving downslope along the north-east direction, is likely originated at the
140 boundary between large boulders and a finer sediment. This layer is in fact characterized by lower resistivities (in t0 $\rho < 10$
141 k Ω m) compared to the shallower depths, and has likely lower permeability. Nevertheless, the presence of large boulders at
142 various depths can lead to funnel flow, and/or splitting of flow paths (Hartmann et al., 2020), which may have determined the
143 infiltration of some injected water upslope (south-west direction) the injection point. From t1 to t5 the negative resistivity
144 variations suggest almost a continuous subsurface flow in the north-east direction along the maximum slope gradient, whereas
145 from t6 to t10 local negative resistivity variations indicate the accumulation of injected water. Most likely these local areas
146 have lower permeability and water may reside there for a longer period.

147 The experiment confirms the assumption that a continuous permafrost layer can act as an aquiclude (Giardino et al., 1992;
148 Krainer et al., 2007) or, if it is discontinuous as in the Sadole rock glacier, as an aquitard (Harrington et al., 2018). Furthermore,
149 the survey confirms the reliability of the steepest gradient method to define the boundary of the frozen layer, and the high
150 heterogeneities (vertical and lateral) in mountain permafrost subsurface, as recently highlighted from continuous core drilling
151 by Phillips et al. (2023). Due to these high heterogeneities, a quantitative analysis regarding hydraulic conductivity just via
152 time-lapse ERT monitoring is very challenging. As highlighted by Mewes et al. (2017) with synthetic analysis and seasonal
153 field measurements, it is unrealistic to define the flow paths of water in mountain permafrost subsurface just via resistivity
154 changes in tomograms. Moreover, the sampling step of the ERT datasets is forced by their acquisition time and may be too
155 large, especially in the initial phases of the experiment. In our case, due to logistical problems (adverse weather), it was not
156 possible to extend the survey measurements for the time necessary to return completely to the pre-injection conditions.

157 Future development of the current work is to perform the experiment in an active rock glacier during late summer, in order to
158 test the flow paths with a fully developed active layer, collecting datasets with a shorter sampling step and for a longer period,
159 until the subsurface system returns completely to the pre-injection conditions. In this way, a possible estimation of hydraulic
160 conductivity in the active layer could be achieved.



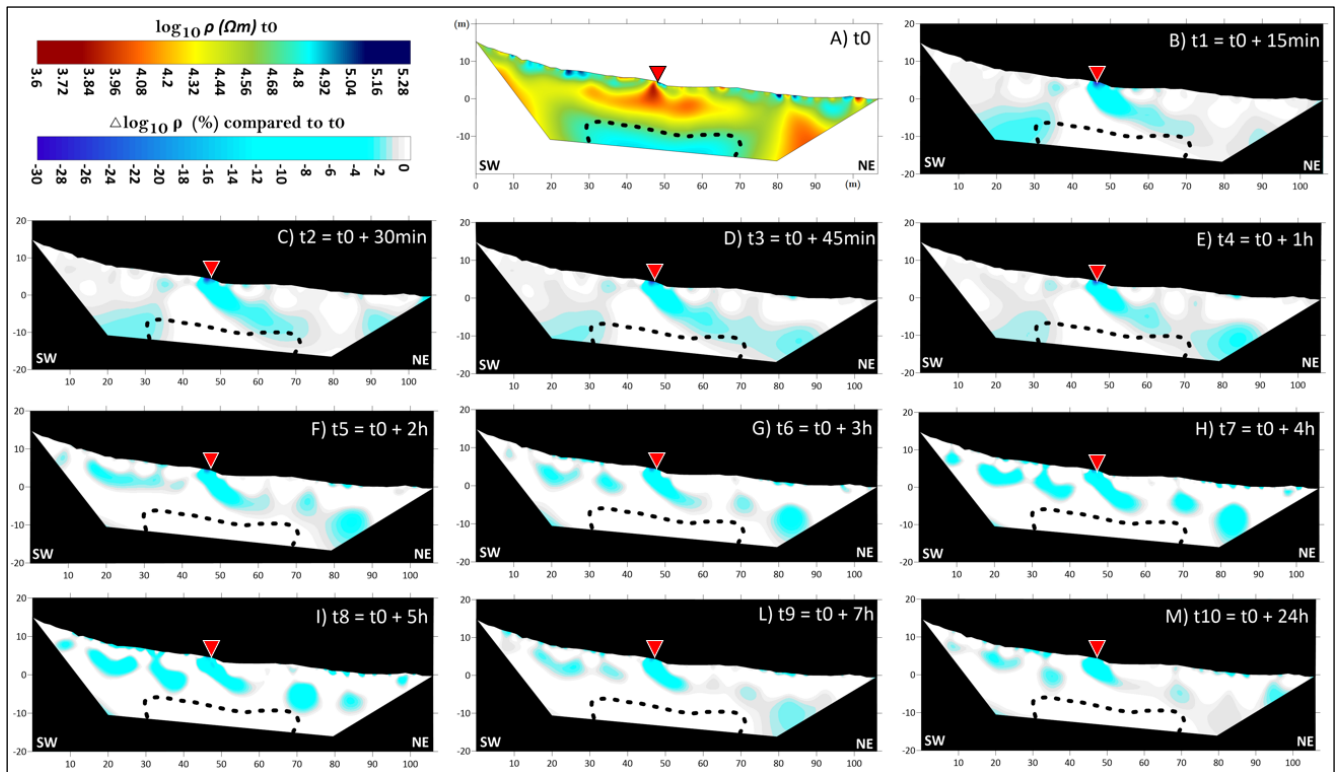
161

162 **Figure 1:** A) Geographic location of the Sadole rock glacier (yellow star), adapted from © Google Earth Pro and Italian Physical
 163 Map produced by The University of Texas at Austin; B) hillshaded LiDAR DEM (modified from WebGIS PAT – Provincia
 164 Autonoma di Trento) showing the three different units that compose the Sadole rock glacier (yellow lines). Blue, violet, and brown
 165 lines represent ERT surveys performed in summer 2021, red circles defines the position of soil temperature sensors, and the green
 166 circle is the location of the Austrian well (1st World War); C) Orthophoto (Commissione Glaciologica SAT, 2022) showing the ERT
 167 transect (red line) used for the infiltration experiment, the salt water injection point (blue star – 1950 m a.s.l.), and the location of
 168 the rock glacier spring (brownish triangle – 1796 m a.s.l.). Blue and violet dashed lines represent ERT surveys performed in 2021
 169 and showed in larger scale in Fig.1B. D) Inverted resistivity section of the blue ERT survey line performed in summer 2021. E)
 170 Inverted resistivity section of the violet ERT survey line performed in summer 2021.



171
 172 **Figure 2: A) Electrodes inserted between the boulders using sponges soaked with saltwater to improve the contact resistances of the**
 173 **ERT surveys; B) 10 bins placed at the selected injection point in early spring 2022, filled with snow and covered with nylon sheets**
 174 **pierced at their center to collect rainwater; C) injection of 800 liters of salt water into the subsurface system.**

175



176
 177 **Figure 3: A) Inverted resistivity section calculated from the t0 dataset. Inverted resistivity variations (%) compared to t0 model,**
 178 **calculated using the logarithmic values, for B) t1 dataset (t0 + 15 minutes), C) t2 dataset (t0 + 30 minutes), D) t3 dataset (t0 + 45**
 179 **minutes), E) t4 dataset (t0 + 1 hour), F) t5 dataset (t0 + 2 hours), G) t6 dataset (t0 + 3 hours), H) t7 dataset (t0 + 4 hours), I) t8 dataset**
 180 **(t0 + 5 hours), L) t9 dataset (t0 + 7 hours), and M) t10 dataset (t0 +24 hours). The black dashed line represents the boundary of the**
 181 **frozen layer defined applying the steepest gradient method to the inverted resistivity model t0. Red triangles represent the injection**
 182 **point of 800 liters of salt-water.**

183

184

185

186 *Author contributing.* MP, JB, AC and MZ were involved in the data acquisition; MP performed the data processing; LC realized
187 the geological framework; GZ carried out the interpretation of the results; all authors contributed to the writing and editing of
188 the manuscript.

189 *Acknowledgements.* Authors thanks: Tommaso and Barbara, managers of “Il rifugio Baita Monte Cauriol”, for the logistical
190 support; the “Magnifica Comunità di Val di Fiemme” and “Comune di Ziano” for authorizing the investigations; and the
191 “Servizio Geologico della Provincia Autonoma di Trento” for the support.

192 *Data Availability Statement.* The datasets used to obtain the results presented in this work are available at the open source
193 repository: <https://zenodo.org/badge/latestdoi/541527187> (DOI: 10.5281/zenodo.7113054).

194 **References**

195 Binley, A: Tools and Techniques: Electrical Methods. In: Gerald Schubert (editor-in chief), Treatise on Geophysics, 2nd
196 edition, Vol 11. Oxford: Elsevier; p. 233-259, <https://doi.org/10.1016/B978-0-444-53802-4.00192-5>, 2015.

197 Blanchy, G., Saneiyani, S., Boyd, J., McLachlan, P., and Binley, A.: ResIPy, an intuitive open source software for complex
198 geoelectrical inversion/modeling. *Computers & Geosciences*, 137, 104423, <https://doi.org/10.1016/j.cageo.2020.104423>,
199 2020.

200 Carturan L., G. Zuecco, R. Seppi, T. Zanoner, M. Borga, A. Carton, and D. Dalla Fontana: Catchment scale permafrost
201 mapping using spring water characteristics. *Permafrost and Periglacial Processes*, 27, 253-270,
202 <https://doi.org/10.1002/ppp.1875>, 2016.

203 Cassiani G., Binley A.M., and Ferre T.P.A.: Unsaturated zone processes. In: Applied Hydrogeophysics (eds H. Vereecken, A.
204 Binley, G. Cassiani, A. Revil and K. Titov), pp. 75–116, Springer Verlag, https://doi.org/10.1007/978-1-4020-4912-5_4, 2016.

205 Cassiani, G., Godio, A., Stocco, S., Villa, A., Deiana, R., Frattini, P., and Rossi, M.: Monitoring the hydrologic behavior of a
206 mountain slope via time-lapse electrical resistivity tomography. *Near Surface Geophysics*, 7(5-6), 475-486,
207 <https://doi.org/10.3997/1873-0604.2009013>, 2009.

208 Chambers, J. E.: Bedrock detection beneath river terrace deposits using three-dimensional electrical resistivity tomography.
209 *602 Geomorphology*, 177–178, 17–25, <https://doi.org/10.1016/j.geomorph.2012.03.034>, 2012.

210 Giardino, J. R., Vitek, J. D., and Demorett, J. L.: A model of water movement in rock glaciers and associated water
211 characteristics. In *Periglacial Geomorphology: Proceedings of the 22nd Annual Binghampton Symposium in Geomorphology*,
212 pp. 159–184, 1992.

213 Harrington, J. S., Mozil, A., Hayashi, M., and Bentley, L. R.: Groundwater flow and storage processes in an inactive rock
214 glacier. *Hydrological Processes*, 32(20), 3070-3088, <https://doi.org/10.1002/hyp.13248>, 2018.

215 Hartmann A., Semenova E., Weiler M., and Blume T.: Field observations of soil hydrological flow path evolution over 10
216 millennia. *Hydrology and Earth System Sciences*, 24, 3271–3288, <https://doi.org/10.5194/hess-24-3271-2020>, 2020.

217 Hauck, C., and Kneisel, C.: *Applied Geophysics in Periglacial Environments*, Cambridge University Press, 2008.

218 Herring, T., and Lewkowicz, A. G.: A systematic evaluation of electrical resistivity tomography for permafrost interface
219 detection using forward modeling. *Permafrost and Periglacial Processes*, <https://doi.org/10.1002/ppp.2141>, 2022.

220 Krainer K., Mostler W., and Spötl C.: Discharge from active rock glaciers, Austrian Alps: a stable isotope approach. *Austrian
221 Journal of Earth Sciences*, 100, 102-112, 2007.

222 Maier F., van Meerveld I., Weiler M. Long-term changes in runoff generation mechanisms for two proglacial areas in the
223 Swiss Alps II: Subsurface flow. *Water Resources Research*, 57, e2021WR030223. DOI:10.1029/2021WR030223, 2021.

224 Mewes, B., Hilbich, C., Delaloye, R., and Hauck, C.: Resolution capacity of geophysical monitoring regarding permafrost
225 degradation induced by hydrological processes, *The Cryosphere*, 11, 2957–2974, <https://doi.org/10.5194/tc-11-2957-2017>,
226 2017.

227 Pauritsch, M., Wagner, T., Winkler, G., and Birk, S.: Investigating groundwater flow components in an Alpine relict rock
228 glacier (Austria) using a numerical model. *Hydrogeology Journal*, 25(2), 371-383, 2017.

- 229 Pavoni, M., Carrera, A., and Boaga, J.: Improving the galvanic contact resistance for geoelectrical measurements in debris
230 areas: a case study. *Near Surface Geophysics*, <https://doi.org/10.1002/nsg.12192>, 2022.
- 231 Phillips, M., Buchli, C., Weber, S., Boaga, J., Pavoni, M., and Bast, A.: Brief communication: Combining borehole
232 temperature, borehole piezometer and cross-borehole electrical resistivity tomography measurements to investigate seasonal
233 changes in ice-rich mountain permafrost, *The Cryosphere*, 17, 753–760, <https://doi.org/10.5194/tc-17-753-2023>, 2023.
- 234 RGIK (2022). Towards standard guidelines for inventorying rock glaciers: baseline concepts (version 4.2.2). IPA Action Group
235 Rock glacier inventories and kinematics, 13 pp.
- 236 Seppi, R., Carton, A., Zumiani, M., Dall' Amico, M., Zampedri, G. and Rigon, R.: Inventory, distribution and topographic
237 features of rock glaciers in the southern region of the Eastern Italian Alps (Trentino). *Geogr. Fis. Dinam. Quat.* 35 (2012), 185-
238 197, <https://doi.org/10.4461/GFDQ.2012.35.17>, 2012.
- 239 Wagner T., Pauritsch M., and Winkler G.: Impact of relict rock glaciers on spring and stream flow of alpine watersheds:
240 examples of the Niedere Tauern Range, Eastern Alps (Austria). *Aust J Earth Sci* 109, <https://doi.org/10.17738/ajes.2016.0006>,
241 2016.